Three-Dimensional Spheroidal Culture Visualization of Membranogenesis of Bruch's Membrane and Basolateral Functions of the Retinal Pigment Epithelium

Rina Sato,[1] *Tsutomu Yasukawa,*[1,2] *Johannes Kacza,*[3] *Wolfram Eichler,*[2] *Akiko Nishiwaki,*[1,2] *Ianors Iandiev,*[2] *Masaharu Ohbayashi,*[1] *Aki Kato,*[1] *Yousef Yafai,*[2] *Andreas Bringmann,*[2] *Ayae Takase,*[1] *Yuichiro Ogura,*[1] *Johannes Seeger,*[3] *and Peter Wiedemann*[2]

Purpose. Aging changes in the RPE involve lipid accumulation and membranous basal deposits onto the underlying Bruch's membrane, which may be related to AMD. Conventional in vitro cell culture is limited in its ability to observe the epithelial functions on the basal side. The purpose of this study was to develop a three-dimensional culture system to observe basolateral functions of the RPE.

Methods. Isolated human RPE cells were cultured in a viscous medium on a rounded-bottom culture dish, resulting in spheroid formation. The appearance and size of the spheroids were assessed by light microscopy. Spheroids were fixed in 4% paraformaldehyde for immunohistochemistry or sampled for Western blotting. For transmission electron microscopy (TEM) and scanning electron microscopy (SEM), spheroids were postfixed in 1% osmium tetroxide.

Results. The spheroids had a differentiated RPE monolayer with a thin elastic layer, a main layer of Bruch's membrane, on their surface and showed outward deposition of lipoproteins with apoB-100. TEM revealed widely spaced collagen, which was identified as condensation of collagen fibrils by SEM. SEM showed deposition of membranous debris and lipid particles, which have been observed in human Bruch's membrane. Western blotting showed expression of RPE differentiation markers and components of Bruch's membrane and RPE lipoproteins.

Conclusions. This model provides direct views of epithelialization processes involving elastogenesis and functions at the basolateral side such as lipoprotein deposition and may elucidate not only unknown epithelial behaviors but also the pathogenesis of RPE-related diseases. (*Invest Ophthalmol Vis Sci.* 2013;54:1740–1749) DOI:10.1167/iovs.12-10068

RPE underlies the neurosensory retina and plays a key role in retinal physiologic functions and pathology in a variety of retinal diseases, including AMD, central serous chorioretinopathy, and RP. AMD is currently a major cause of irreversible vision loss among elderly individuals in most industrialized nations.[1–3] Aging changes in and under the RPE cells are thought to be closely associated with the pathogenesis of AMD.[4,5] Genetic alteration of the retinoid cycle regulated by the photoreceptor and RPE cells may result in some forms of RP.[6] Thus, the RPE is essential for maintaining retinal function. However, not all RPE functions, such as maintenance of Bruch's membrane and transmural transport and deposition of lipoproteins and debris in the direction of the choriocapillaris, an outer vascular plexus, have been clarified.

Bruch's membrane has five layers: the basement membrane of the RPE, the inner collagenous layer, the elastic layer, the outer collagenous layer, and the basement membrane of the choriocapillaris.[5] Age-related changes in Bruch's membrane include thickening, thinning, decreased integrity of the elastic layer, decreased hydraulic conductivity, and accumulation of cholesterol and other lipids, advanced glycation products, and membranous deposits.[4,5,7–9] Extracellular basal deposits between the RPE and Bruch's membrane, referred to as drusen for localized types or basal laminar and linear deposits for diffuse types, also involve lipids. Large drusen are thought to be risk factors for exudative AMD.[10,11] Thus, lipids that accumulate under the RPE are likely to play a key role in the pathogenesis of AMD. The origin of the accumulated lipids may be the RPE, because it produces and deposits lipoproteins with apoB-100 in the direction of Bruch's membrane.[12–16] Nevertheless, while the behavior of deposition of lipoproteins as large as 20 to 200 nm in diameter should accompany the remodeling (maintenance) of Bruch's membrane, the synchronized functions of the RPE for transmural deposition of lipoproteins and remodeling of Bruch's membrane have not been fully clarified. To understand ocular aging and the pathogenesis of AMD, clarifying unknown basolateral functions and events among the RPE, Bruch's membrane, and choriocapillaris may be necessary.

Conventional in vitro culture has critical limitations for discerning the epithelial functions of the RPE. RPE cells, once isolated from eyes, tend to lead to dedifferentiation and transdifferentiation into myofibroblasts especially in culture with serum, characterized by decreased intracellular components of cytokeratin and increased smooth muscle actin (SMA)

From the [1]Department of Ophthalmology and Visual Science, Nagoya City University Graduate School of Medical Sciences, Nagoya, Japan; and the Departments of [2]Ophthalmology and [3]Anatomy, Histology, and Embryology, University of Leipzig, Leipzig, Germany.

Supported by German Research Community (DFG) grant WI 880/9-1 and by a 2006 Grant-in-Aid for Scientific Research No. 18591929 from Japan Society for the Promotion of Science.

Submitted for publication April 22, 2012; revised October 2 and December 3, 2012; accepted December 8, 2012.

Disclosure: **R. Sato**, None; **T. Yasukawa**, None; **J. Kacza**, None; **W. Eichler**, None; **A. Nishiwaki**, None; **I. Iandiev**, None; **M. Ohbayashi**, None; **A. Kato**, None; **Y. Yafai**, None; **A. Bringmann**, None; **A. Takase**, None; **Y. Ogura**, None; **J. Seeger**, None; **P. Wiedemann**, None

Corresponding author: Tsutomu Yasukawa, Department of Ophthalmology and Visual Science, Nagoya City University Graduate School of Medical Sciences, 1 Kawasumi, Mizuho-cho, Mizuho-ku, Nagoya 467-8601, Japan; yasukawa@med.nagoya-cu.ac.jp.

Investigative Ophthalmology & Visual Science, March 2013, Vol. 54, No. 3

fibers.[17,18] Therefore, many studies have evaluated RPE cells based only on the primary culture and/or culture with serum-free medium. However, the basolateral side of the RPE cells should be exposed initially to serum derived from the choriocapillaris. Transwell culture is a unique and excellent method to enhance the formation of tight junctions among the RPE cells.[19–23] It is easy to change the content of the culture medium at the apical and basal sides and is superior for evaluating the polarity of RPE cells. However, a culture plate may mechanically limit the functions at the basal side of the RPE and their observation. Alternatively, ARPE-19, an RPE cell line, is often used for in vitro experiments.[19] However, the cell line may have abnormal morphogenesis regarding epithelial formation and may require no adhesion to the extracellular matrix to survive.

A multicellular spheroid culture system was developed, originally to enhance differentiation and tube formation of vascular endothelial cells,[24] and, thereafter, it was applied to a coculture system.[25] This system has advantages for culturing the endothelium or epithelium in that it can form a differentiated monolayer on the surface of the spheroids. We found that, because the RPE has the fundamental function of continuous phagocytosis of the photo-oxidized tips of the outer segments of the photoreceptor cells, the spheroids of the RPE cells could remain viable, possibly through phagocytosis of inner material derived from apoptotic cells and subsequent outward deposition of lipoproteins similar to the physiologic condition in eyes. We report a novel culture system of RPE cells using multicellular spheroids, representing redifferentiation, re-epithelialization, and formation of Bruch's membrane. This culture showed that the spheroids deposit lipoproteins through Bruch's membrane. This model may be useful to elucidate the as yet unclarified basolateral functions of the RPE and the pathogenesis of AMD and other RPE-related diseases.

Methods

Cell Culture

Human tissue was used in accordance with applicable laws and the Declaration of Helsinki for research. Tissues were used after patients provided written informed consent, according to procedures approved by the ethics committee of Leipzig University Medical School. Human retinal pigment epithelial (HRPE) cells were obtained from several donors within 48 hours of death and prepared as described previously.[26] Alternatively, HRPE cells were purchased from the supplier (Lonza Walkersville, Inc., Walkersville, MD). HRPE cells that were shipped were cryopreserved primary RPE cells that had been packaged at passage 2 and that contained 500,000 or more cells per vial. The cells were suspended in Ham F-10 medium containing 10% fetal bovine serum, diagnostic medium (Glutamax II; Invitrogen, Tokyo, Japan), and gentamicin and were cultured in tissue culture flasks (Greiner, Tokyo, Japan) in 95% air/5% CO_2 at 37°C. The cells from passages 3 to 6 were used. The epithelial nature of the RPE cells was routinely identified by immunocytochemistry using the monoclonal antibodies AE1 (which recognizes most acidic type I keratins) and AE3 (which recognizes most basic type II keratins); both were obtained from Chemicon (Hofheim, Germany). All tissue culture components and solutions were purchased from Gibco BRL (Paisley, Scotland).

Preparation of Spheroids

The HRPE cell spheroids were generated with minor modification according to the protocol described previously.[24] Briefly, stock methylcellulose solution was prepared by dissolving 6 g of methylcellulose (Sigma-Aldrich, Munich, Germany) in 500 mL of Ham F-10 medium and collecting the supernatant by centrifugation. After conventional culture on the culture plate, the HRPE cells were trypsinized, collected, and centrifuged. Then, 2250, 4500, or 6750 HRPE cells were resuspended in 150 μL of culture medium with 20% stock methylcellulose solution (v/v) in nonadherent 96-well culture plates with a rounded bottom (Nunc, Langenselbold, Germany). After 7 days of culture, the spheroids were harvested and cultured further, if necessary, with 15 mL of culture medium in nonadherent 10-cm culture dishes.

Spheroid Size

RPE spheroids were observed by light microscopy. The diameter of the RPE spheroids was measured under a light microscope with a scale on days 1, 7, 14, 28, and 56. The measurement was done using 32 spheroids from each time point and was repeated three times.

Cell Viability of RPE Spheroids

On days 1, 7, 14, 28, and 56, the spheroids were collected and forwarded to a tetrazolium-based colorimetric assay (XTT assay) to determine cell numbers. The RPE spheroids were transferred onto 96-well cell culture plates (Iwaki Glass, Tokyo, Japan), and 50 μL of the XTT solution was added to the culture. After another 4-hour incubation, the absorbance at 450 nm was determined by spectrophotometry (model DU-64; Beckman Instruments, Tokyo, Japan). Each experiment was performed using eight wells and was repeated four times.

Terminal Deoxynucleotidyl Transferase (TdT)-Mediated dUTP Nick-End Labeling (TUNEL) Assay

The samples were fixed with 4% paraformaldehyde in 0.1 M PBS for 20 minutes at room temperature and then were washed three times with PBS. Subsequently, they were cryoprotected by infiltration with successive solutions of 10, 20, and 30% sucrose in PBS at 4°C. The samples were embedded in Tissue-Tek optimum cutting temperature compound (OCT; Sakura Finetek, Tokyo, Japan) and then were frozen in dry ice–ethanol. Specimens were sectioned at 10 μm (CM1850 cryostat; Leica Microsystems K.K., Tokyo, Japan), and the consecutive sections were collected on slides and air-dried for 30 minutes.

The sections then were incubated in a permeabilization solution containing 0.1% Triton X-100 in PBS for 30 minutes at 4°C. A TUNEL assay was performed using an ApoMark DNA Fragmentation Detection Kit (Exalpha Biologicals, Inc., Shirley, MA), according to the manufacturer's instructions. For negative control purposes, TdT enzyme was omitted from the reaction mixture. As a positive control, sections were treated with DNase I (Takara Bio Inc., Otsu, Japan), which stained all nuclei. All spheroid sections were observed on differential interference contrast images under a Provis AX-70 microscope (Olympus, Tokyo, Japan). Images were processed using DP controller (Olympus) and Photoshop CS6 software (Adobe Systems Inc., San Jose, CA).

Immunohistochemical Analysis

For whole-mount immunostaining, spheroids with 4500 HRPE cells seeded were used. The spheroids were harvested and fixed for 5 minutes in 0.2 M PBS (pH 7.8) containing 4% paraformaldehyde. After fixation, the spheroids were washed five times with Tris-buffered saline containing 1 mM $CaCl_2$ (TBS-Ca) (pH 7.6). The spheroids then were transferred back into TBS-Ca with 0.1% Triton X and treated with 2% H_2O_2 at 4°C for 4 hours to diminish endogenous peroxidase reactivity. After washing, the spheroids were incubated with primary antibodies at 4°C overnight. The primary antibodies used were polyclonal goat anti-occludin (1:100; Santa Cruz Biotechnology, Heidelberg, Germany), monoclonal mouse anti-collagen type I (1:200; Calbiochem, Darmstadt, Germany), monoclonal mouse anti-collagen type IV (1:200; Calbiochem), and rabbit anti-elastin (1:200;

Table 1. Profile of Protein Expression in RPE Spheroids

Proteins	Primary Antibodies			
	Purpose	Host	Dilution	Supplier
Differentiation markers				
Occludin	WB, IHC	Rabbit	250	Abcam, Cambridge, MA
ZO-1	WB, IHC	Rabbit	50	Abcam, Cambridge, MA
RPE65	WB	Mouse	500	Abcam, Cambridge, MA
Bestrophin	WB	Rabbit	500	Calbiochem, La Jolla, CA
Cytokeratin 18	WB, IHC	Mouse	1000	Sigma, Saint Louis, MO
Bruch's membrane components				
Collagen type I	WB	Rabbit	500	Abcam, Cambridge, MA
Collagen type IV	WB	Rabbit	500	Abcam, Cambridge, MA
Elastin	WB	Rabbit	50	Acris, Herford, Germany
Lipoprotein components				
apoB-100	WB	Rabbit	1000	Calbiochem, La Jolla, CA
apoA-I	IHC	Rabbit	1000	BioVision, Mountain View, CA
apoE	WB	Rabbit	500	Abcam, Cambridge, MA

WB, Western blotting; IHC, immunohistochemistry.

Calbiochem). The staining procedure was carried out according to the protocol of the Pathostain ABC-POD (M) kit (Wako, Osaka, Japan). The spheroids were treated for 10 minutes with Hoechst 33258 (Sigma-Aldrich) after fixation to stain the nuclei. Samples were observed using a light microscope (Axioplan 2; Carl Zeiss Meditec, Jena, Germany). Immunofluorescence microscopy was performed on Zeiss Axiovert200M with AxioCamMRc5 (Carl Zeiss). Digitized images were analyzed and measured with the concomitant image-analysis software (Axiovision; Carl Zeiss). Microscopic panels were composed using Adobe Photoshop C53.

BODIPY Staining of Lipid Droplets

The spheroids were fixed with 4% paraformaldehyde in 0.1 M PBS for 20 minutes. The specimens then were washed three times with PBS for 10 minutes. Lipid droplets were stained with BODIPY 493/503 (D3922; Molecular Probes, Carlsbad, CA) (stock concentration, 1 mg/mL; working solution, 1:1000 dilution) for 20 minutes at room temperature. The samples were then placed again on a glass-bottom dish mounted in an antifade medium with 4′,6-diamidino-2-phenylindole (DAPI) to stain nulei (Vectashield; Vector Laboratories, Burlingame, CA). The samples were analyzed under a Zeiss LSM laser confocal microscope (Carl Zeiss, Oberkochen, Germany). Images were processed using Photoshop CS6 software (Adobe Systems Inc.).

Ultrastructural Analysis

For electron microscopy, the spheroids were harvested and fixed for 60 minutes in 0.2 M PBS with 2.5% glutaraldehyde and 4% paraformaldehyde. After washing, the spheroids were inserted into LUMiTainer, spherical microcontainers (obtained from KG Lerche, Berlin, Germany). For transmission electron microscopy (TEM), the spheroids were postfixed in 1% osmium tetroxide in 0.1 M PBS for 1 hour, dehydrated in graded ethanol series up to 100%, embedded in epoxy resin (Nisshin EM Co. Ltd., Tokyo, Japan), trimmed, and cut into ultrathin sections. Thin sections were stained with 2% uranyl acetate and lead citrate and were imaged on a Zeiss 900 electron microscope or a JEM-2000EX TEM (JEOL Co. Ltd., Tokyo, Japan). For scanning electron microscopy (SEM), the LUMiTainer shell was removed after the drying process, and the spheroids were placed on adhesive tape on top of the SEM stubs. Specimens were sputter coated with gold palladium 90/10 (30 mA at 5×10^{-2} mbar for 40 seconds with a 50-mm target–specimen distance) and were observed by SEM.

Western Blotting

The extracts of the spheroids were prepared using mammalian protein extraction reagent (M-PER; Pierce, Rockford, IL) supplemented with protease inhibitors. An equal amount of protein (15 or 30 μg) and molecular weight markers were resolved by SDS-PAGE (10%) and were transferred to polyvinylidene difluoride membranes (Immobilon-P; Millipore, Billerica, MA). Blocking was done for 1 hour with 3% BSA (Sigma-Aldrich) in 50 mM Tris-Cl, pH 7.5, 150 mM NaCl, 0.2% Triton X-100 (TS buffer). Mouse monoclonal anti-SMA antibody (1:1000; Dako), or other primary antibodies (Table 1) were diluted with TS buffer containing 1% BSA and were incubated with membranes overnight at 4°C. After washing six times with TS containing 0.5% BSA (washing buffer), the membranes were incubated for 1 hour with horseradish peroxidase conjugated secondary antibody (50 ng/mL). The antibody was removed by washing six times with washing buffer. Finally, the sample was stained with SuperSignal West Pico substrate (Pierce). The visualized images were scanned with a chemiluminescence imaging analyzer (Fluo Chem; Alpha Innotech, Santa Clara, CA). For normalization purposes, the membranes were reprobed with a rabbit polyclonal anti-glyceraldehyde 3-phosphate dehydrogenase antibody (Cell Signaling Technology, Tokyo, Japan) or a SMA antibody.

Results

Reproducibility of Spheroid Culture

One day after initiation of the spheroid culture, the cell suspensions slowly sank in the viscous medium and aggregated to form a spherical mass. A monolayer of RPE formed on the surface of the spherical mass (Figs. 1A–D). Regarding size and cell viability, the process of spheroid formation was highly reproducible and depended on the number of cells seeded. Spheroids were made with 2250, 4500, and 6750 cells, corresponding to 1:2:3 in volume. Therefore, the theoretical ratio of diameter should be 1:1.26:1.44 (the cubic root of 1:2:3). The actual ratio of the diameter of the spheroids with the initial cell numbers of 2250, 4500, and 6750 was 1:1.25:1.42, which corresponded to that of the theoretical diameter (Table 2). The size gradually decreased for 4 weeks and reached a plateau (Figs. 1A–E). The decrease in size was time dependent and was independent of the number of cells seeded (Fig. 1E). For the 4 weeks during which the size decreased, outward deposition of material was observed. In

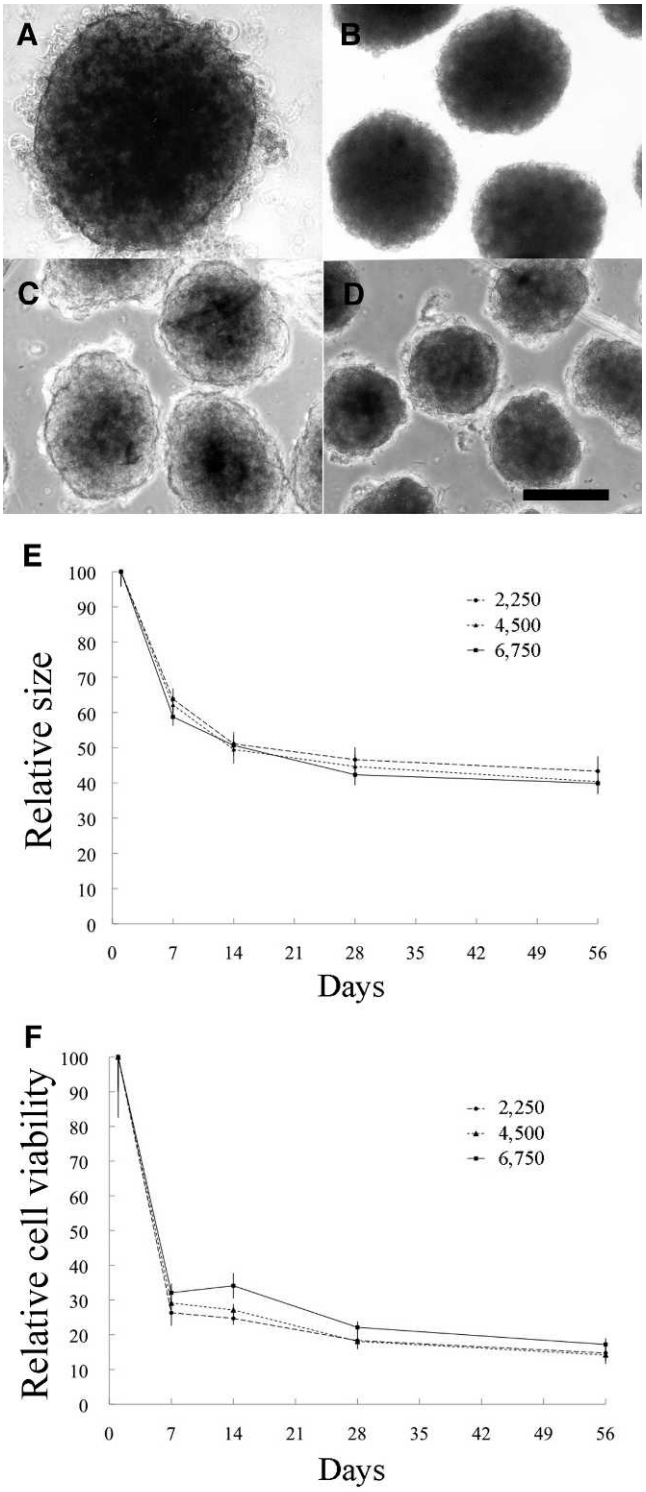

Figure 1. Appearance and cell viability of spheroids. Light microscopic images of RPE spheroids on days 1 (**A**), 7 (**B**), 14 (**C**), and 56 (**D**) (**A**, **C**, **D**, phase contrast; **B**, bright-field microscopic image). *Scale bar* = 100 μm. (**E**) Temporal changes in the mean diameters of spheroids made from 2250, 4500, or 6750 RPE cells. The data are expressed as a percentage of the initial (day 1) mean diameter. The diameters gradually decreased for 4 weeks and reached a plateau. The decrease in size is independent of the number of cells seeded. (**F**) Temporal changes in cell viability of spheroids on XTT assay made from 2250, 4500, or 6750 RPE cells. The data are expressed as a percentage of the initial (day 1) value. The cell viability decreased rapidly by 1 week, reached a plateau, and decreased slightly after 2 weeks.

contrast, cell viability rapidly decreased at week 1 by 26.3 to 32.1% of the value on day 1 (Fig. 1F). Thereafter, cell viability reached a plateau and then decreased gradually after 2 weeks. Since cell viability should be correlated to surface surviving cells, the ratio of cell viability of each sized spheroid should be theoretically 1:1.59:2.08 (the square of the cubic root of 1:2:3). The actual ratio of cell viability of the spheroids with the initial cell numbers of 2250, 4500, and 6750 was 1:1.57:1.99, which corresponded to that of the theoretical surface area (Table 2). Actual diameters and cell viabilities are similar to theoretical values, suggesting that the methods might be highly reproducible. Since the cell viability was reflected by the number of surviving cells, RPE cells constructing a monolayer on the surface of the spheroids were likely to remain alive. The decreasing rate of cell viability was time dependent and was minimally affected by the number of cells seeded (Fig. 1F).

Redifferentiation of RPE Cells as an Epithelium in Spheroid Culture

One day after culturing HRPE cells suspended with F10 containing methylcellulose and 10% fetal bovine serum in 96-well, rounded-bottom culture plates, a spheroid formed in each well, with a monolayer of HRPE cells on its surface and a core of disorganized cells (Fig. 2). Apoptosis was observed in a core of disorganized cells. Immunostaining with occludin antibody and TEM showed the morphology of polygonal HRPE cells with tight and gap junctions. Western blotting showed expression of differentiation markers involving occludin, ZO-1, RPE65, bestrophin, and cytokeratin 18 (Figs. 2H, 3; Table 1).

To confirm the status of differentiation of RPE on spheroids, we examined the expression of α-SMA and cytokeratin 18 (Fig. 3). In conventional culture on a flat dish, the expression of cytokeratin 18, a marker of differentiated RPE cells, decreased markedly in the HRPE cells, whereas the expression of myoid marker, α-SMA, increased with passage. In contrast, the spheroid culture led to prompt recovery of cytokeratin 18 expression, independent of the passage number. Inversely, the expression of α-SMA decreased. These results indicated that once HRPE cells were cultured as spheroids, even trans-differentiated HRPE cells were promptly redifferentiated.

Bruch's Membrane-like Structure Generated on the Spheroid Surface

Essentially all RPE cells joined to form a spheroid, which was packed into a round shape by lamellipodial crawling onto the outermost surface within a day (Figs. 4A–C). Thereafter, a thin membrane with elastin coated the spheroids (Figs. 4D–F). The generated outer membranous structure of the spheroids was sometimes stripped off the spheroids artificially during immunohistochemistry (Figs. 4G, 4H). Western blotting showed expression of collagen types I and IV and elastin (Fig. 4I; Table 1). These extracellular matrix proteins, which are also elements of native Bruch's membrane, diffusely covered the spheroids. The basement membrane comprised of collagen IV formed between the RPE and the reticular lamina of the elastin (Fig. 4F).

TEM and SEM were performed to view Bruch's membrane-like structure generated on the surface of the spheroids (Figs. 4, 5). SEM also showed a collagenous and elastic layer on the outermost side of the spheroids. TEM demonstrated that elastin-packed granules were translocated and assembled into the lamellipodia, disintegrated, and linked to form a reticular layer (Figs. 5A–H). SEM showed that the long-spaced collagen observed on TEM possibly represented collagen fibrils deposited from basal infolding of the HRPE cells (Figs. 5I–N). The fibrils were assembled and flattened and formed the basal

Table 2. Relationship of the Number of Seeded Cells to the Diameter and Cell Viability of RPE Spheroids

No. of Cells Seeded	2250	4500	6750
Average ratio of diameter (range)	1.00	1.25 (1.20–1.29)	1.42 (1.36–1.50)
Average ratio of cell viability (range)	1.00	1.57 (1.47–1.69)	1.99 (1.67–2.30)
Theoretical ratio of diameter	1.00	1.26	1.44
Theoretical ratio of surface area	1.00	1.59	2.08
Theoretical ratio of volume	1.00	2.00	3.00

lamina of the RPE. The ultrastructures of the basal lamina and the collagenous and elastic layer (Fig. 4F) were similar to that of human Bruch's membrane observed with the quick-freeze/deep-etch method, which showed greater detail than conventional TEM.[27]

Extracellular Deposition of Lipoproteins

Extracellular deposition of lipoproteins was observed in the culture of the RPE spheroids (Fig. 6). Light microscopy disclosed granular deposits on the surface of the spheroids (Figs. 6A, 6B). SEM showed that these deposits were comprised primarily of nanoparticles, 120 to 250 nm in diameter (Fig. 6H). Deposits were positively stained by BODIPY and were observed, especially until week 3, to be correlated with expression of apoB-100. These findings suggested that the nanoparticles were lipoproteins, as observed in human Bruch's membrane, and that these lipoproteins with apoB-100 were produced by RPE cells.

Western blotting showed that RPE lipoproteins consisted of apoB-100, apoE, and apoA-1 (Fig. 6I; Table 1), which was consistent with the results that Li and colleagues report.[13]

Discussion

To date, no systems have provided a three-dimensional view of the structure on the basal side of the RPE. In vitro, bFGF-including medium, the primary culture, and a transwell culture dish can enhance differentiation of the RPE. However, cells cultured on a culture plate should be affected physicochemically and biologically by substrates on the plate, and the plate itself should interfere with observation of the basal side of the epithelium. In vivo, the basal structure should be connected to the underlying choriocapillaris and connective tissue and be observable only by performing a technique to separate them by use of alcohol treatment,[28] NaCl,[29] digestive enzymes,[30] EDTA,[31] or dithiothreitol[32]; by freezing and thawing[33]; or by a quick-freeze/deep-etching method.[27] With all procedures, the visible interstitial surface and the visual field are limited. In contrast, the spheroid system allowed visualization of any interstitial surface without the need to separate the tissue and showed only epithelial cell–derived matrices, such as components of Bruch's membrane and lipoproteins. This in vitro system also enabled direct light microscopic observation of the basal side of the epithelium and immunohistochemical evaluation.

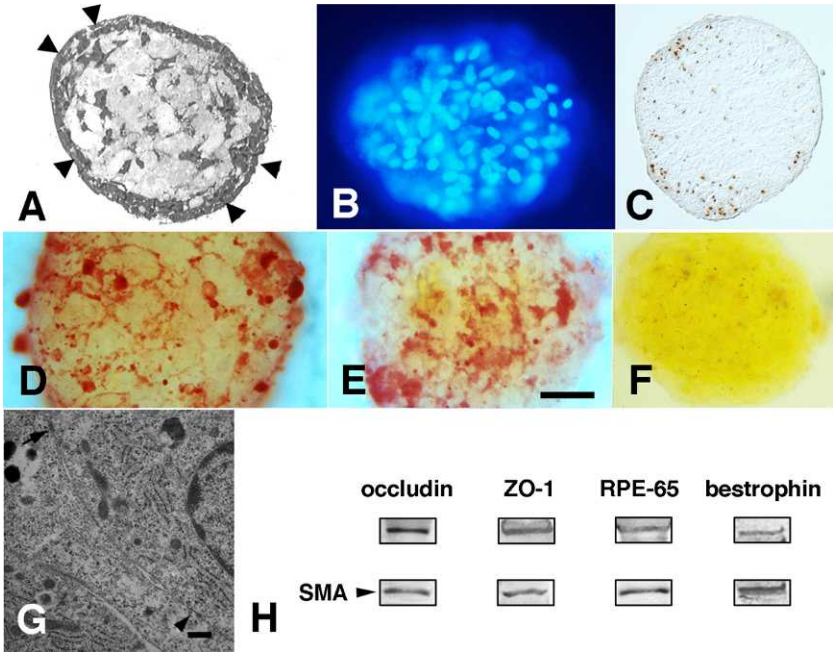

Figure 2. Epithelialization of RPE cells in spheroid culture at week 1. (**A**) A section of a spheroid shows a surface monolayer of RPE cells (*arrowheads*) and a core of disorganized cells. (**B**) Nuclei of a whole-mount spheroid are stained with Hoechst 33258. (**C**) Apoptotic cells detected by TUNEL assay. Apoptosis is detectable in a core of disorganized cells. (**D**, **E**) Expression of occludin (**D**) and cytokeratin 18 (**E**) is observed partially indicating the margin of RPE cells located on the surface of whole-mount spheroids (*scale bar* = 50 μm). (**F**) Negative control shows no specific staining. (**G**) TEM shows electron-dense strands indicative of tight junctional cell–cell contacts (*arrow*) and gap junction (*arrowhead*) (*scale bar* = 500 nm). (**H**) Western blotting shows the expression of specific markers of RPE involving occludin, ZO-1, RPE-65, and bestrophin. SMA levels were measured as a loading control.

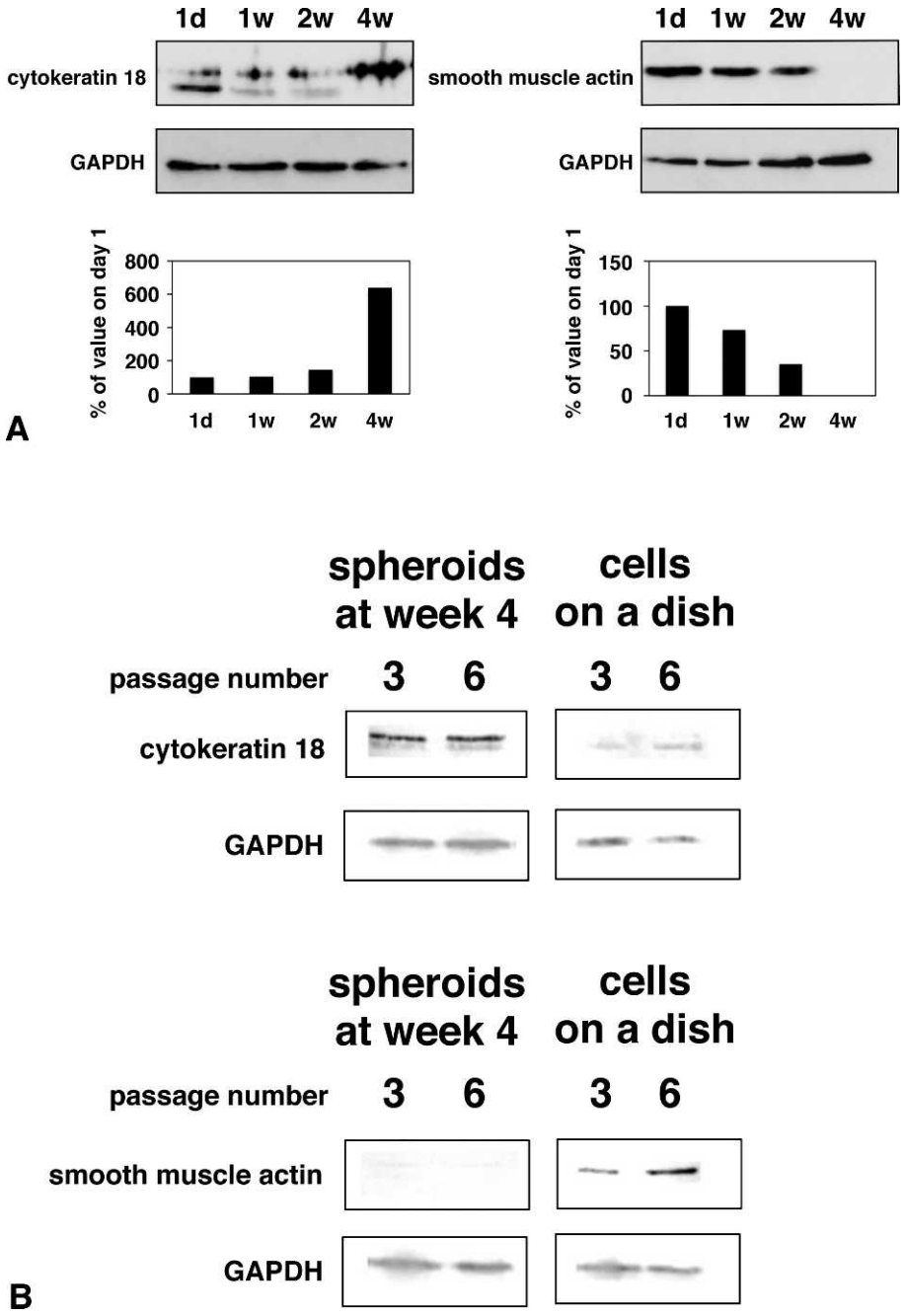

Figure 3. Expression of cytokeratin 18 and smooth muscle actin (SMA) by RPE spheroids. (**A**) The expression of cytokeratin 18 in RPE spheroids increases over time. In contrast, the expression of SMA is barely detectable by week 4. These figures are representative of three different experiments that showed similar results. The *bar graph* represents relative band intensity. (**B**) In conventional culture on a dish, RPE cells tend to have decreased expression of cytokeratin 18 and increased SMA with passages. In contrast, RPE spheroids in any passage recover differentiated characteristics at week 4, expressing cytokeratin 18 but not SMA. Glyceraldehyde-3-phosphate dehydrogenase levels were measured as a loading control.

The status of differentiation and dedifferentiation of HRPE cells is represented by a shift of specific markers involving α-SMA and cytokeratins. α-SMA is a major component of microfilaments essential for contractile activity and is supposed to be a marker of the RPE phenotype with myoid transdifferentiation.[17,18] The phenotype change may substantially contribute to development of proliferative vitreoretinopathy. The dedifferentiated state is also a disadvantage when transplanting HRPE cells to treat AMD.[34] However, cytokeratin 18 is a typical marker for differentiated RPE cells.[17] Cytokeratins are intermediate filaments that are characteristic of epithelial cells. Routinely cultured HRPE cells on tissue culture plastic tend to be transdifferentiated into myofibroblast-like cells with repeated passages and to express α-SMA predominantly to cytokeratins.[17] In contrast, the current study showed that, once HRPE cells were cultured in the multicellular spheroid system, the nature of the RPE as an epithelium resumed with expression of cytokeratin 18, independent of the number of passages (Fig. 3). We speculated that prompt cell–cell contact in the multicellular spheroid system may enhance

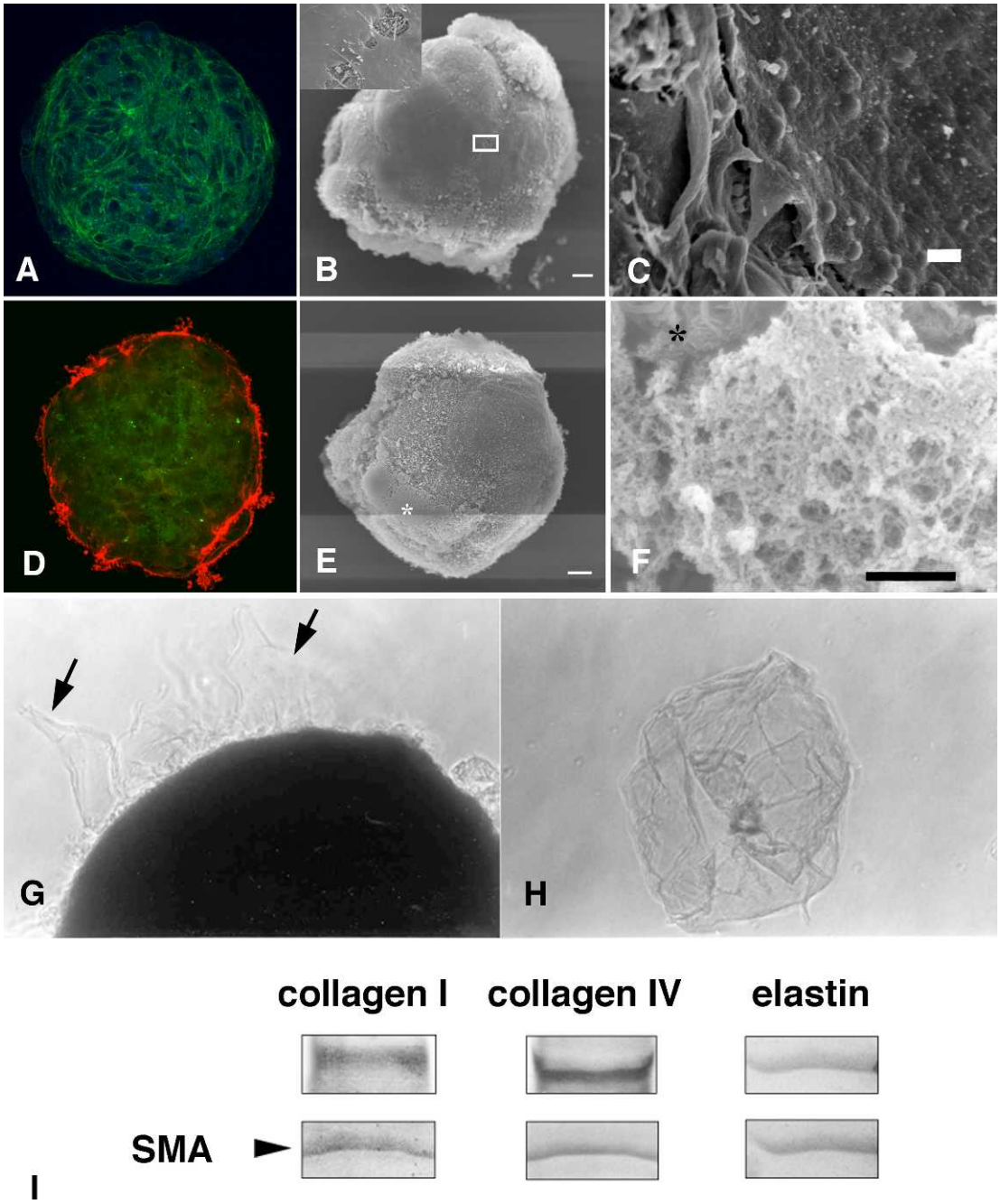

FIGURE 4. Spheroid formation of RPE cells. Appearance of a standard spheroid of RPE cells on day 1 (**A–C**) and at week 4 (**D–F**). (**A**) Actin fibers cover a RPE spheroid, running beyond underlying individual cells (*green*; phalloidin-FITC binding to actin). (**B**) SEM reveals the smooth surface of the spheroids in the early stage. *Inset*: Magnified image in the area indicated by a rectangle. Basal infoldings composed of basal microvilli of RPE cells are visible behind the lamellipodia covering the spheroid surface. (**C**) Lamellipodia on the surface of the spheroids. (**D**) A thin elastic layer covers a RPE spheroid with maturation (*red*, Cy 3 channel). (**E**) The SEM image shows collagenous and elastic layers (*asterisk*). (**F**) Magnified image of the collagenous and elastic layer, which are major elements of Bruch's membrane. Collagen fibrils deposited from the basal microvilli (*asterisk*, see Fig. 5J) are seen behind the elastic and collagenous layer. (**G–I**) Formation of Bruch's membrane on RPE spheroids at week 4. (**G**) A RPE spheroid with partially stripped Bruch's membrane (*arrows*). (**H**) The appearance of the entire Bruch's membrane detached completely from a spheroid. (**I**) Western blotting shows the expression of the extracellular matrix proteins. SMA levels were measured as a loading control. *Bars*: (**B**, **E**) 10 μm; (**C**, **F**) 1 μm.

redifferentiation, while cell–extracellular matrix adhesion may be essential for organized cells to survive.

Lamellipodial crawling may play a critical role in the initial step of spheroid formation. First, a contractile force by actin stress fibers may promote roundly packed shaping of spheroids. Distribution of actin filaments on Figure 4A suggested lamellipodial crawling onto the outermost surface of spheroids as well as cytoskeletons of underlying RPE cells.[35] We found that the threshold of the minimal size of spheroids at formation was small as 100 μm in diameter. That may support the hypothesis that lamellipodial crawling may be essential for spherical formation, because a contractile force must work

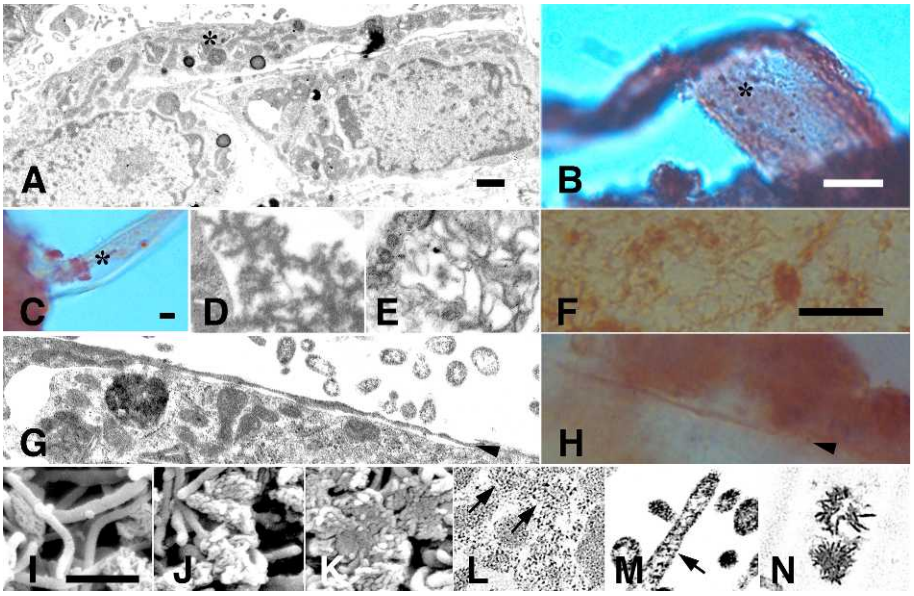

Figure 5. Ultrastructural analysis of a RPE spheroid at week 1. (**A–H**) Formation of the elastic layer. TEM shows elastin-packed granules in the lamellipodia on the surface of a spheroid (*asterisk* in **A**). Immunostaining against elastin shows these granules localized in the lamellipodium, which was artificially stripped from a spheroid in **B** (*asterisk*). Immunostaining against an irrelevant primary antibody (as a negative control) shows no staining in the lamellipodia (*asterisk* in **C**). The granules have disintegrated into reticular formation of elastic fibers (**D–F**) and a thin elastic layer (*arrowheads* in **G** and **H**). (**I–N**) SEM and TEM show the process of formation of the basal lamina of the RPE. Collagen fibrils are deposited from the basal microvilli, flattened, and polymerized with one another, forming a basal lamina of RPE. Long-spaced collagen on TEM (*arrows*) may represent a cross-sectional image of these collagen fibrils. *Bars*: (**B**, **C**, **F**) 10 μm; (**A**, **I**) 1 μm.

tangentially. High reproducibility of spheroid formation was independent of passage number and cell sources. Moreover, induced pluripotent stem cell–derived RPE cells also form a spheroid, expressing α-SMA on its surface (Tsutomu Yasukawa, oral communication, 2013). Therefore, we speculated that not contaminated fibroblasts but RPE cells themselves may play a role in this step. Second, lamellipodia may provide intracellular and intercellular closed spaces to effectively form the elastic layer and the basal lamina, respectively (Figs. 4F, 5). Elastin granules observed in the lamellipodia are supposed to be premature, because they are observed in patients with a fibulin-5 mutation, which plays a critical role in the formation of the elastic fiber. Elastic fibers may be formed through integration of secreted elastin and microfibrils.[36] Thus, dedifferentiation of RPE cells on culture plates represents the behavior of wound healing with the original aim of Bruch's membranogenesis. Nevertheless, further studies are needed to determine the factors that maintain or change the phenotype of the HRPE cells. This spheroid model may be useful to address this issue, possibly resulting in the elucidation of the pathogenesis of proliferative vitreoretinopathy and a breakthrough in transplantation therapy using RPE cells.

Immunohistochemical and SEM observation showed that spheroids of the HRPE cells had basal infolding and had components of Bruch's membrane, including the basement membrane of RPE, the collagenous layers, and the elastic layer (Figs. 4, 5). Long-spaced material running in a parallel fashion and varying in periodicity from 100 to 140 nm was observed in the basal laminar deposits between the plasma membrane and the basement membrane of the RPE in aging eyes or even between the outer collagenous layer and the basal lamina of the choriocapillaris in young eyes.[5,37] This material, widely believed to be derived from collagen IV or VI, has been termed fibrous or long-spaced collagen.[5,38–40] However, controversy remains about whether it is actually comprised of collagen derivatives and whether it has any relevance to AMD, because previous speculation was based only on sectional findings on TEM. We first visualized long-spaced collagen three-dimensionally (Figs. 5I–N). This suggested that it is derived from bundled short collagen fibrils that were densely polymerized with one another and subsequently formed the basal lamina and that long-spaced collagen in the basal laminar deposits in aging eyes and close to the basal lamina of the choriocapillaris in young eyes is produced by RPE cells and choroidal endothelial cells, respectively. Clinically, laser photocoagulation and invasion of the choroidal neovascularization must accompany the breach in Bruch's membrane. In addition, an RPE detachment occurring in some eyes with AMD represents separation of the RPE and Bruch's membrane. In these situations, reformation of Bruch's membrane is required to maintain adjacent retinal functions. This model may be useful to understand the morphogenesis of Bruch's membrane.

Understanding the aging changes in the RPE and Bruch's membrane is important to clarify the pathogenesis of AMD. The spheroids comprised only of RPE cells may clarify the roles of RPE cells in lipid accumulation in Bruch's membrane, drusen biogenesis, and other pathologies in AMD. Lipid particles, 80 to 200 nm in diameter, have been observed increasingly with advancing age in Bruch's membrane, basal linear deposits, and drusen.[8,9,41] Malek et al. report that RPE cells might secrete apoB-100, although it has been widely thought to be produced only in the liver.[12] However, the possibility that the protein detected by Western blotting might have been derived from serum contaminating cell lysate could not be excluded in their experiment. In the current study, local deposits observed by light microscopy involved lipid droplets, and SEM showed lipid particles 120 nm or larger in diameter. Western blotting showed expression of apoE, apoA-I, and apoB-100 (Fig. 6), which supported the idea that RPE produces lipoproteins possessing apoB-100 and other specific apolipoproteins, as Li et al. suggest.[13] Thus, the current results strongly suggested that the lipid nanoparticles in Bruch's membrane in aging eyes originate mainly from the RPE cells. In addition, this important new finding suggested that HRPE cells

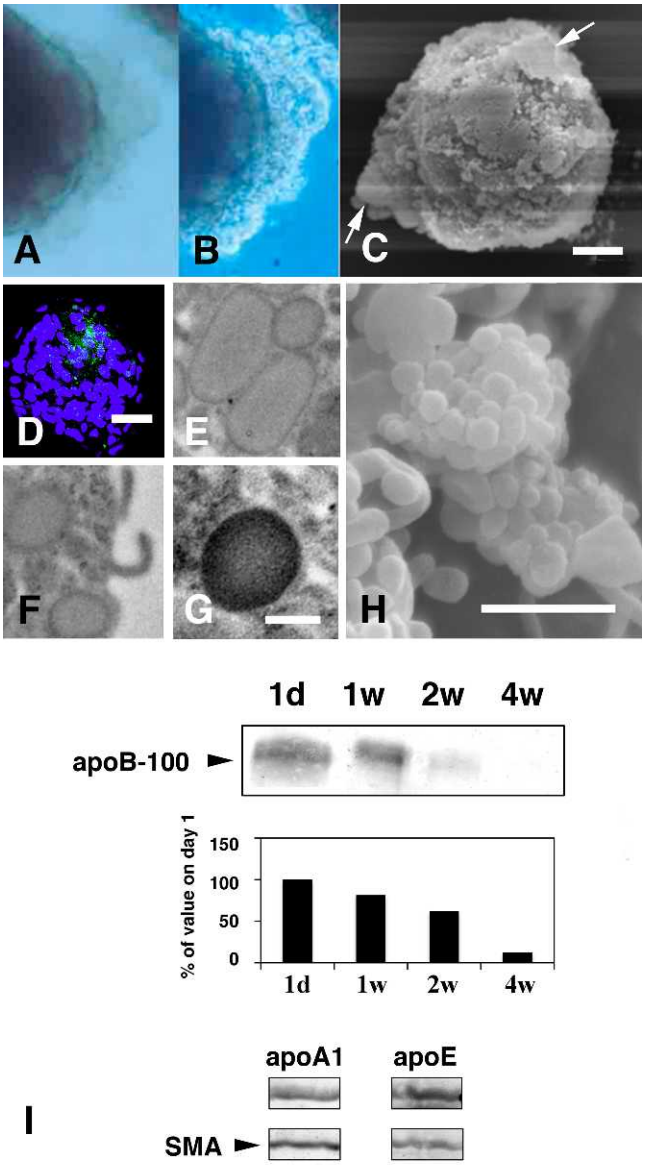

Figure 6. Deposition of lipoproteins from RPE spheroids. (**A**, **B**) Conventional light microscopy shows RPE-deposited material (**A**, bright-field image; **B**, phase-contrast microscopic image). (**C**) SEM on a spheroid at week 2 shows deposits (*arrows*) and a collagenous membrane complex. (**D**) BODIPY staining shows lipid droplets (*green*). Nuclei were stained with DAPI (*blue*). Magnified images on TEM (**E–G**) and SEM (**H**) show lipid particles with a diameter of 120 nm or larger, and lipid droplets, which are comparable to those deposited in Bruch's membrane in aging human eyes. (**I**) Western blotting shows that the spheroids express apoB-100, apoA1, and apoE, which are components of RPE lipoproteins. The *bar graph* represents the relative band intensity. The time course of expression of apoB-100 is correlated with the amount of the deposits on spheroids and expression of SMA (Fig. 2A). Bands of apoA1 and apoE are from samples of spheroids at week 1. *Bars*: (**C**) 20 μm; (**D**) 50 μm; (**E–G**) 0.5 μm; (**H**) 1 μm.

may produce lipoproteins even under physiologic conditions. We speculated that the origin of the lipoproteins deposited by RPE cells may be phagocytosed cellular membranes, because the decreasing size of the spheroids was synchronized with the lipoprotein depositions (Figs. 1E, 6I). In human eyes, the RPE phagocytoses photo-oxidized tips of the outer segments of the photoreceptors, whereas a surface monolayer of RPE spheroids may phagocytose the center of the apoptotic cells. The phagocytosis of the center of the apoptotic cells by a surface spheroid RPE possibly resulted in the decreasing size of the spheroids, while the total cell viability of the spheroids, mainly derived from the surface RPE, was relatively stable over time (Fig. 1). The phagocytic activity on the spheroids should be investigated in a future study. The initial size of the spheroids is highly reproducible, dependent on the number of RPE cells seeded. Temporal profiles of size and cell viability are also reproducible but are based on epithelial functions and are minimally affected by the initial number of cells. These findings suggested that events on the spheroids occur during the physiologic state. Thus, three-dimensional spheroid culture may simulate physiologic behaviors of the RPE. A decrease in the size and deposition of lipoproteins larger than 120 nm should accompany remodeling of Bruch's membrane. In fact, the time course of the decrease in the size of spheroids and the expression of apoB-100 were correlated with the expression of α-SMA (Figs. 3, 6).

In conclusion, multicellular spheroid culture of HRPE cells is suitable for enhancing redifferentiation and observing Bruch's membrane formation and extracellular deposition of lipoproteins toward the basolateral side. In aging eyes, Bruch's membrane has accumulated lipid deposits and other debris, which are likely to be part of the pathogenesis of AMD. Therefore, spheroid culture of RPE cells may be helpful to understand the manner by which Bruch's membrane is maintained and lipoproteins are deposited and to elucidate the mechanism of aging in eyes and the pathogenesis of AMD and other RPE-related diseases. Spheroid culture may provide substantial information to determine the as yet unknown general functions of the epithelium.

Acknowledgments

We thank Ute Weinbrecht, Karin Bartholomäus, and Silke Jantzen for technical assistance. Tsutomu Yasukawa conducted the current study as an Alexander von Humboldt Foundation scholar.

References

1. Friedman DS, O'Colmain BJ, Munoz B, et al. Prevalence of age-related macular degeneration in the United States. *Arch Ophthalmol*. 2004;122:564–572.
2. Mitchell P, Smith W, Attebo K, Wang JJ. Prevalence of age-related maculopathy in Australia. The Blue Mountains Eye Study. *Ophthalmology*. 1995;102:1450–1460.
3. Klein R, Klein BEK, Linton KLP. Prevalence of age-related maculopathy. The Beaver Dam Eye Study. *Ophthalmology*. 1992;99:933–943.
4. Killingworth MC. Age-related components of Bruch's membrane in the human eye. *Graefes Arch Clin Exp Ophthalmol*. 1987;225:406–412.
5. Guymer R, Luthert P, Bird A. Changes in Bruch's membrane and related structures with age. *Prog Retin Eye Res*. 1999;18:59–90.
6. Lamb TD, Pugh EN Jr. Dark adaptation and the retinoid cycle of vision. *Prog Retin Eye Res*. 2004;23:307–380.
7. van der Schaft TL, Mooy CM, de Bruijn WC, Oron FG, Mulder PG, de Jong PT. Immunohistochemical light and electron microscopy of basal laminar deposit. *Graefes Arch Clin Exp Ophthalmol*. 1994;232:40–46.
8. Haimovici R, Gantz DL, Rumelt S, Freddo TF, Small DM. The lipid composition of drusen, Bruch's membrane, and sclera by hot stage polarizing light microscopy. *Invest Ophthalmol Vis Sci*. 2001;42:1592–1599.

9. Curcio CA, Millican CL. Basal linear deposit and large drusen are specific for early age-related maculopathy. *Arch Ophthalmol*. 1999;117:329–339.
10. Bressler SB, Maguire MG, Bressler NM, Fine SL. The Macular Photocoagulation Study Group. Relationship of drusen and abnormalities of the retinal pigment epithelium to the prognosis of neovascular macular degeneration. *Arch Ophthalmol*. 1990;108:1442–1447.
11. Klein R, Klein BE, Jensen SC, Meuer SM. The five-year incidence and progression of age-related maculopathy: the Beaver Dam Eye Study. *Ophthalmology*. 1997;104:7–21.
12. Malek G, Li C, Guidry C, Medeiros NE, Curcio CA. Apolipoprotein B in cholesterol-containing drusen and basal deposits of human eyes with age-related maculopathy. *Am J Pathol*. 2003;162:413–425.
13. Li CM, Clark ME, Chimento MF, Curcio CA. Apolipoprotein localization in isolated drusen and retinal apolipoprotein gene expression. *Invest Ophthalmol Vis Sci*. 2006;47:3119–3128.
14. Wang L, Li CM, Rudolf M, et al. Lipoprotein particles of intraocular origin in human Bruch membrane: an unusual lipid profile. *Invest Ophthalmol Vis Sci*. 2009;50:870–877.
15. Wu T, Fujihara M, Tian J, et al. Apolipoprotein B100 secretion by cultured ARPE-19 cells is modulated by alteration of cholesterol levels. *J Neurochem*. 2010;114:1734–1744.
16. Curcio CA, Johnson M, Rudolf M, Huang JD. The oil spill in ageing Bruch membrane. *Br J Ophthalmol*. 2011;95:1638–1645.
17. Grisanti S, Guidry C. Transdifferentiation of retinal pigment epithelial cells from epithelial to mesenchymal phenotype. *Invest Ophthalmol Vis Sci*. 1995;36:391–405.
18. Zheng Y, Bando H, Ikuno Y, et al. Involvement of rho-kinase pathway in contractile activity of rabbit RPE cells in vivo and in vitro. *Invest Ophthalmol Vis Sci*. 2004;45:668–674.
19. Dunn KC, Aotaki-Keen AE, Putkey FR, Hjelmeland LM. ARPE-19, a human retinal pigment epithelial cell line with differentiated properties. *Exp Eye Res*. 1996;62:155–169.
20. Holtkamp GM, Van Rossem M, de Vos AF, Willekens B, Peek R, Kijlstra A. Polarized secretion of IL-6 and IL-8 by human retinal pigment epithelial cells. *Clin Exp Immunol*. 1998;112:34–43.
21. Zhang N, Kannan R, Okamoto CT, Ryan SJ, Lee VH, Hinton DR. Characterization of brimonidine transport in retinal pigment epithelium. *Invest Ophthalmol Vis Sci*. 2006;47:287–294.
22. Sonoda S, Spee C, Barron E, Ryan SJ, Kannan R, Hinton DR. A protocol for the culture and differentiation of highly polarized human retinal epithelial cells. *Nat Protoc*. 2009;4:662–673.
23. Johnson LV, Forest DL, Banna CD, et al. Cell culture model that mimics drusen formation and triggers complement activation associated with age-related macular degeneration. *Proc Natl Acad Sci U S A*. 2011;108:18277–18282.
24. Korff T, Augustin HG. Integration of endothelial cells in multicellular spheroids prevents apoptosis and induces differentiation. *J Cell Biol*. 1998;143:1341–1352.
25. Korff T, Kimmina S, Martiny-Baron G, Augustin HG. Blood vessel maturation in a 3-dimensional spheroidal coculture model: direct contact with smooth muscle cells regulates endothelial cell quiescence and abrogates VEGF responsiveness. *FASEB J*. 2001;15:447–457.
26. Enzmann V, Kaufmann A, Hollborn M, Wiedemann P, Gemsa D, Kohen L. Effective chemokines and cytokines in the rejection of human retinal pigment epithelium (RPE) cell graft. *Transpl Immunol*. 1999;7:9–14.
27. Ruberti JW, Curcio CA, Millican CL, Menco BP, Huang J, Johnson M. Quick-freeze/deep-etch visualization of age-related lipid accumulation in Bruch's membrane. *Invest Ophthalmol Vis Sci*. 2003;44:1753–1759.
28. Browning AC, Shah S, Dua HS, Maharajan SV, Gray T, Bragheeth MA. Alcohol debridement of the corneal epithelium in PRK and LASEK: an electron microscopic study. *Invest Ophthalmol Vis Sci*. 2003;44:510–513.
29. Mihara M, Miura M, Suyama Y, Shimano S. Scanning electron microscopy of the epidermal lamina densa in normal human skin. *J Invest Dermatol*. 1992;99:572–578.
30. Overton J. Response of epithelial and mesenchymal cells to culture on basement lamella observed by scanning microscopy. *Exp Cell Res*. 1977;105:313–323.
31. Holmstrup P, Dabelsteen E, Harder F. EDTA separation and recombination of epithelium and connective tissue of human oral mucosa. *Expl Cell Biol*. 1985;53:32–40.
32. Osawa T, Feng XY, Nozaka Y. Scanning electron microscopic observations of the basement membranes with dithiothreitol separation. *Med Electron Microsc*. 2003;36:132–138.
33. Osawa T. The localization of laminin, fibronectin, and lectin-binding sites on the epidermal basal lamina. *J Electron Microsc*. 1986;35:259–271.
34. Sheridan C, William R, Grierson I. Basement membranes and artificial substrates in cell transplantation. *Graefes Arch Clin Exp Ophthalmol*. 2004;242:68–75.
35. Campos M, Amaral J, Becerra SP, Fariss RN. A novel imaging technique for experimental choroidal neovascularization. *Invest Ophthalmol Vis Sci*. 2006;47:5163–5170.
36. Hu Q, Loeys BL, Coucke PJ, et al. Fibulin-5 mutations: mechanisms of impaired elastic fiber formation in recessive cutis laxa. *Hum Mol Genet*. 2006;15:3379–3386.
37. van der Schaft TL, de Bruijn WC, Mooy CM, Ketelaars DA, de Jong PT. Is basal laminar deposit unique for age-related macular degeneration? *Arch Ophthalmol*. 1991;109:420–425.
38. Knupp C, Munro PM, Luthert PK, Ezra E, Squire JM. Structure of abnormal molecular assemblies (collagen VI) associated with human full thickness macular holes. *J Struct Biol*. 2000;129:38–47.
39. Knupp C, Chong NH, Munro PM, Luthert PJ, Squire JM. Analysis of the collagen VI assemblies associated with Sorsby's funds dystrophy. *J Struct Biol*. 2002;137:31–40.
40. Reale E, Groos S, Eckardt U, Eckardt C, Luciano L. New components of 'basal laminar deposits' in age-related macular degeneration. *Cells Tissues Organs*. 2009;190:170–181.
41. Curcio CA, Millican CL, Bailey T, Kruth HS. Accumulation of cholesterol with age in human Bruch's membrane. *Invest Ophthalmol Vis Sci*. 2001;42:265–274.